Use of the Left Ventricular Time-Activity Curve as a Noninvasive Input Function in Dynamic Oxygen-15-Water Positron Emission Tomography

Hidehiro Iida, Christopher G. Rhodes, Ranil de Silva, Luis I. Araujo*, Peter M. Bloomfield, Adriaan A. Lammertsma, and Terry Jones

MRC Cyclotron Unit, Hammersmith Hospital, London, United Kingdom

Noninvasive recording of arterial input functions using regions of interest (ROIs) in the left ventricular (LV) chamber obviates the need for arterial cannulation in PET, but it is compromised by the limited recovery coefficient of the LV chamber and by statistical noise. In the present study, a new mathematical model has been developed, which corrects for the spillover of radioactivity both from the myocardium into the LV ROI and the blood into the myocardial ROI. The method requires the measurement of a time-activity curve in the LV chamber during the dynamic $H_2{}^{15}O$ PET study and the measurement of the recovery coefficient of the LV ROI using a ^{15}O-carbon monoxide ($C^{15}O$) scan and venous blood sampling. This approach was successfully validated against direct measurements of the arterial input function using an on-line beta detector in five greyhounds undergoing dynamic $H_2{}^{15}O$ PET imaging. This technique also yielded myocardial blood flow (MBF) values which were not significantly different from those obtained with the beta-probe analyses (maximum difference <2%), provided that the LV ROIs were sufficiently large to provide good counting statistics. When this model was not applied for large ROIs (small recovery in LV ROI), systematic overestimations in MBF compared with beta-probe analysis (e.g., a factor by 40% for a recovery coefficient of 0.7) were observed. Thus, this technique enabled the prediction of an accurate input function using the LV time-activity curve, and hence, noninvasive quantification of MBF without arterial cannulation.

J Nucl Med 1992; 33:1669–1677

Positron emission tomography (PET) has the ability to quantitatively determine physiological function in vivo. This is based on the accurate measurement of the radiotracer concentration in arterial blood (the input function) and in tissue (the tissue response). Measurement of the arterial input function is performed either by sampling at discrete times via a cannulated artery (*1*) or by continuously withdrawing blood to monitor the arterial radioactivity curve (*1,2*). In cardiac PET, noninvasive determination of the input function without arterial cannulation may be provided by measuring the time-activity curve of a region of interest (ROI) positioned over the cardiac chamber (left ventricle, LV, or left atrium, LA) of dynamically-acquired PET images (*3*). However, the following limitations to this approach exist:

1. The ROI time-activity curve obtained from the cardiac chamber includes statistical fluctuations due to limited counting statistics, especially when data are collected with high temporal resolution. This could amplify statistical variation and systematic errors in calculated functional parameters, in particular when measuring myocardial blood flow (MBF) using ^{15}O-water (*4–6*).
2. The measured counts in the ROI are underestimated due to the limited recovery coefficient, which is caused by the finite spatial resolution of PET cameras and cardiac motion.
3. The noninvasive arterial time-activity curve may also include spillover contamination from myocardial tissue radioactivity.

The latter two factors could cause systematic errors in the measurement of MBF.

The purpose of the present study was to establish a method which overcomes the three limitations described above. A new model has been developed that corrects for issues 2 and 3. This model allows for the use of a relatively large ROI (or severe smoothing operation) and hence maximizes the available count statistics in the noninvasive input function. The method is an extension of a previously described technique (*2*), which only corrected for limited recovery of radioactivity in tissue.

MATERIALS AND METHODS

Theory

Definitions of the symbols used in this model are listed in Table 1. In deriving the model, the following assumptions were

Received Jun. 14, 1991; revision accepted Apr. 13, 1992.

For reprints contact: Dr. Hidehiro Iida, DSc, Research Institute for Brain and Blood Vessels, Akita 6-10 Senshu-Kubota-Machi, Akita City, Akita, 010 Japan.

* Current address: Division of Nuclear Medicine, Department of Radiology, Hospital of the University of Pennsylvania, Philadelphia, PA.

made:

1. The tissue radioactivity concentration following the administration of $H_2{}^{15}O$ is described by a conventional single-compartment model (*7,8*):

$$C_i(t) = f \cdot a(t) \otimes e^{-f/p \cdot t}. \quad \text{Eq. 1}$$

2. MBF distribution is homogeneous throughout the left ventricular myocardial wall, and radioactivity concentration in a selected LV ROI, $LV(t)$, is described by:

$$LV(t) = \beta \cdot a(t) + \gamma \cdot \rho \cdot C_i(t). \quad \text{Eq. 2}$$

3. The measured radioactivity concentration in a selected myocardial ROI, $R(t)$, is described by:

$$R(t) = \alpha \cdot f \cdot a(t) \otimes e^{-f/p \cdot t} + V_a \cdot a(t). \quad \text{Eq. 3}$$

4. A component of spillover of tissue radioactivity into the LV ROI is the residual of the recovery coefficient of the LV:

$$\beta + \gamma = 1. \quad \text{Eq. 4}$$

Solving Equations 1, 2, 3 and 4 gives

$$R(t) = \left(\frac{\alpha}{\beta} - \frac{(1-\beta)}{\beta^2} \cdot \rho \cdot V_a\right) \cdot f \cdot LV(t) \otimes e^{-(1/p+(1-\beta)/\beta \cdot \rho) \cdot f \cdot t} + \frac{V_a}{\beta} \cdot LV(t) \quad \text{Eq. 5}$$

and

$$a(t) = \frac{1}{\beta} \cdot LV(t) - \frac{(1-\beta)}{\beta^2} \cdot \rho \cdot f \cdot LV(t) \otimes e^{-(1/p+(1-\beta)/\beta \cdot \rho) \cdot f \cdot t}. \quad \text{Eq. 6}$$

The values of MBF (f),the tissue fraction (α) and the arterial blood volume (V_a) can be estimated by nonlinear least squares regression analysis of the measured myocardial and LV ROI time-activity curves to Equation 5. The value of β is measured separately using a blood volume scan (see data analysis), and the values of p (partition coefficient of water) and ρ (density of the myocardium) are fixed at a value of 0.91 ml/g (*4*) and 1.04 g/ml (*9*), respectively. The true input function can be calculated from Equation 6 using the calculated values of f, α and V_a together with given values of β and p.

Simulation Studies

A simulation study was performed to evaluate the effects of the limited recovery of the LV counts (i.e., $\beta < 1.0$) on the MBF values calculated from the dynamic $H_2{}^{15}O$ PET data. First, a myocardial curve $R(t)$ was calculated according to Equation 3 using an assumed input function, $a(t)$. In this simulation, the following parameters were fixed: $f = 1.0$ ml/min/g, $\alpha = 0.6$ g/ml, $V_a = 0.3$ ml/ml and p = 0.91 ml/g. Second, using the same parameters, LV curves, $LV(t)$s, were generated according to Equation 2 for different values of the recovery coefficient (β) within the range 0.6 to 1.0. The effect of distortion in $LV(t)$ as compared with the true input function was assessed by fitting $R(t)$ to Equation 3 using $LV(t)$ as the input function rather than the directly measured input function $a(t)$. Then, the difference between the fitted and the initial values of MBF, α and V_a, was examined as a function of the recovery coefficient of the LV counts (β). Simulations were performed for two kinds of input function (Fig. 1): first, an arterial curve such as that observed in a typical greyhound study during a 3.5-min $C^{15}O_2$ inhalation and second, a curve obtained in a human study with a bolus injection of $H_2{}^{15}O$.

A second simulation was performed to evaluate effects of statistical noise in the input function on calculated values of f, α and V_a. The same myocardial tissue curve $R(t)$ and the input curve $a(t)$ as described above were also used in this simulation. Statistical noise was added to each data point (1 sec interval) of the assumed input function by generating Gaussian random numbers for various noise levels. The noise level was defined as the standard deviation at the peak of the input function. For each noise level, 500 noise-added input functions were generated, where the magnitude of the fluctuation at each data point was determined so that the standard deviation was proportional to the square-root of the absolute counts (Fig. 2). Each input function was binned according to the scan sequence of the PET study (see below) to provide the LV time-activity curves. Three parameters, f, α and V_a, were fitted, and subsequently, the fluctuation and systematic bias in the calculated parameters were estimated for each noise level.

A third simulation was performed to evaluate the effect of errors in the measured values of the recovery coefficient of the LV (β) on calculated values of f, α and V_a. First, the myocardial tissue curve, $R(t)$, and the LV curve, $LV(t)$, were generated by assuming the same parameters as mentioned above with $\beta = 0.7$. Second, values of f, α and V_a were calculated by changing the assumed beta value from −40% to +40%. Then, the difference of the calculated parameters from the assumed values were estimated for each β value.

TABLE 1
Definitions of Symbols

$Ci(t)$	True myocardial tissue radioactivity concentration at time t; radioactivity per gram of perfusable myocardium (cps/g).
$a(t)$	True input function; radioactivity concentration per milliliter of blood (cps/ml).
$R(t)$	Time-activity curve of radioactivity per milliliter of ROI which is selected in the myocardial region (cps/ml).
$LV(t)$	Time-activity curve of radioactivity per milliliter of ROI which is selected in the LV region (cps/ml).
f	Regional MBF; the flow per gram of perfusable tissue (ml/min/g).
p	Myocardium-to-blood partition coefficient of water (ml/g).
α	Tissue fraction; grams of perfusable tissue per milliliter of ROI (g/ml).
V_a	Arterial blood volume; milliliters of arterial vascular space (including the spillover from the chamber) per milliliter of ROI (ml/ml).
β	Recovery coefficient of left-ventricular ROI ($0.0 < \beta \leq 1.0$).
γ	Spillover fraction of tissue radioactivity into LV ROI ($0.0 \leq \gamma < 1.0$).
ρ	Myocardial tissue density (1.04 g/ml).

Note: All radioactivity concentrations are corrected for decay.

Animal Preparation

Five greyhounds (28–33 kg) were sedated with 4 mg intramuscular acetapromazine after overnight fasting. Anesthesia was induced with intravenous pentobarbital sodium (25 mg/kg). Ani-

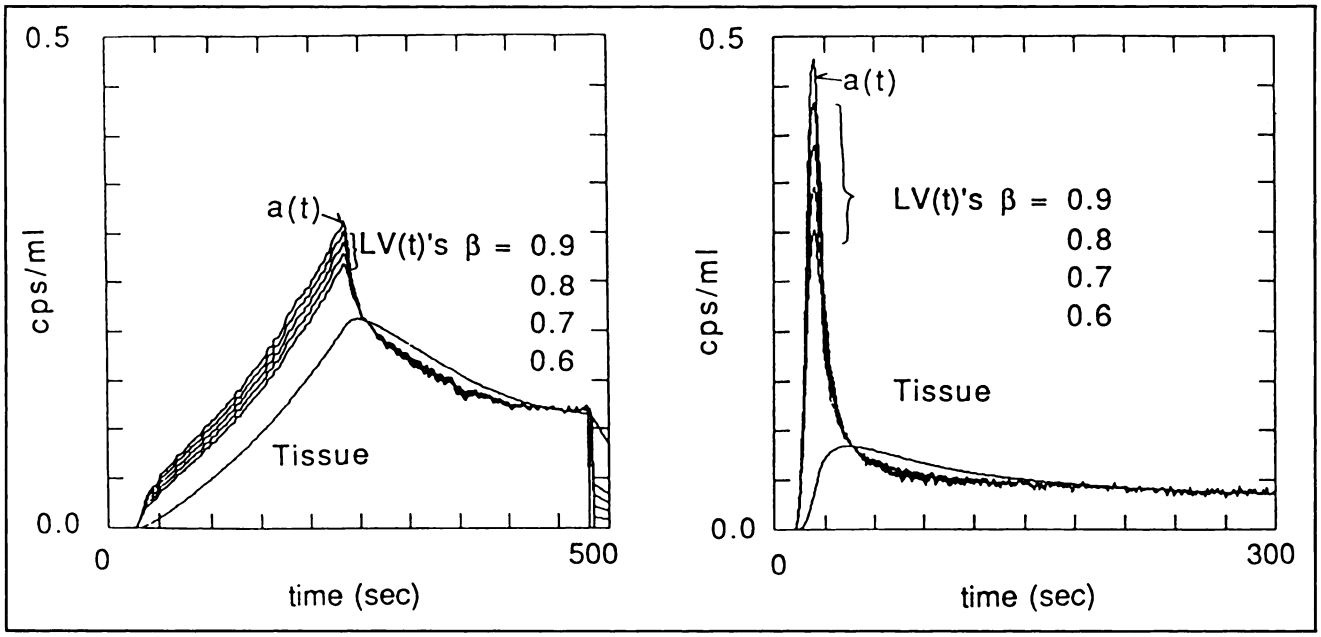

FIGURE 1. Assumed input functions and simulated LV time-activity curves for (A) slow and (B) bolus $H_2{}^{15}O$ administration protocols. The input functions are indicated by the solid lines which have the highest peak in each figure. The slow input function was obtained from a typical study using 3.5 min continuous inhalation of gaseous $C^{15}O_2$, and the bolus input function by a typical study using an intravenous bolus injection of ^{15}O-water. Both input functions were used for the simulations. The curves indicated by the lowest peak in each figure correspond to the tissue time-activity curves calculated by the equation: $\rho \cdot f \cdot a(t) \otimes e^{-f/\rho \cdot t}$. Values of f = 1.0 ml/min/g and ρ = 0.91 ml/g were assumed to simulate these tissue curves. The $LV(t)$ curves in both panels were calculated according to Equation 2 for various assumed values of the recovery coefficient (β). All curves were decay-corrected to time zero.

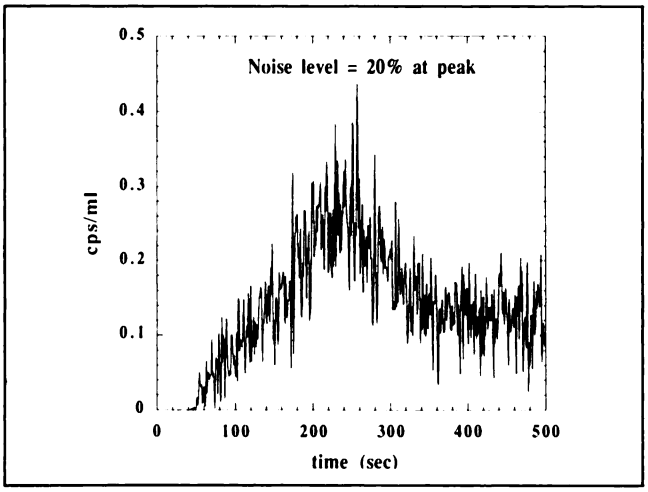

FIGURE 2. An example of a noise-added input function with a noise level of 20%. The statistical noise was added to each data point (1-sec interval). This curve was binned according to each scan duration of a given scan sequence described in the text to simulate the LV time-activity curves. The simulated LV curves were used in the simulation to estimate effects of statistical noise in the input function on the calculated values. Five hundred independent input functions were generated at each noise level, 10%, 20%, 30%, 50% and 60%. The noise level denotes the standard deviation of the Gaussian distribution at the peak of the input function. Magnitude of the noise at other time points was determined so that the standard deviation at each data point was proportional to the square-root of the expected absolute counts at each time point.

mals were intubated and mechanically ventilated with a mixture of oxygen, air and nitrous oxide. Anesthesia was maintained by inhalation of 0.5–1% of halothane.

Catheters were placed in the left femoral artery and vein. Arterial blood was continuously withdrawn at flow rate of 5 ml/min and the radioactivity concentration was measured using a plastic scintillator (beta probe) (*1,2*). The withdrawn blood was returned to the animal through the venous catheter. Arterial blood pressure, electrocardiogram and arterial blood gases were monitored throughout the procedure.

PET

All PET studies were performed using an ECAT 931-08/12 tomograph (CTI Inc., Knoxville, TN), which enables 15 planes of data acquisition over an axial field of view (FOV) of 10.5 cm (*10*). All emission and transmission data were reconstructed using a Hanning filter with a cut-off frequency of 0.5 in units of the reciprocal of the sampling interval of the projection data (3.07 mm). This reconstruction resulted in an in-plane spatial resolution of 8.4 ± 0.7 mm FWHM for emission data and 7.7 ± 0.7 mm FWHM for transmission data (*11*) at the center of the FOV. The axial resolution was 6.6 mm FWHM at the center of the FOV.

After positioning the dog in the left lateral decubitus position, a 5-min rectilinear scan was performed by exposure of a $^{68}Ge/^{68}Ga$ ring source in order to determine the optimal imaging position. A 20-min transmission scan was then performed by exposure of the same $^{68}Ge/^{68}Ga$ ring source in order to correct subsequent emission data for tissue attenuation of 511 keV annihilation gamma photons. For the blood-pool measurement,

a 6-min emission scan was initiated 1 min after a 4-min inhalation of $C^{15}O$ (total supply of 6 GBq). Seven venous blood samples were collected at 1-min intervals during the scan, and the whole blood $C^{15}O$ concentration was measured using a NaI well counter cross-calibrated with the scanner.

After a 15-min period to allow for the decay of ^{15}O radioactivity to background levels, MBF was measured according to a previously validated protocol (*5*). Briefly, $C^{15}O_2$ was inhaled for a period of 3.5 min at a concentration of 3–5 MBq/ml and a flow rate of 500 ml/min. A 24 frame dynamic PET scan was started at the beginning of the $C^{15}O_2$ delivery which comprised six frames each of 5, 10, 20 and 30 sec duration.

Beta-Probe Curve

The beta-probe curves were corrected for delay and dispersion of the tracer through the beta-probe tubing and for deadtime losses of the detector electronics. The degree of dispersion was determined independently by measuring the response to a step function input and was corrected by assuming the dispersion function to be a single exponential function (*2*). The measured dispersion time constant for the present system was 5.0 sec.

The deadtime losses of the detector electronics were corrected according to the equation:

$$N_{true} = \frac{1}{1 - \Delta t \cdot N_{meas}} N_{meas}, \qquad \text{Eq. 7}$$

where N_{true} is the true counting rate corrected for the deadtime (cps), N_{meas} the measured counting rate, and Δt the deadtime of the system (sec). Deadtime was evaluated empirically by sequential counting of a ^{15}O-solution and was found to be 1.5 μsec. The maximum correction was approximately 5%.

Data Analysis

All images were reconstructed on a MicroVax II computer (Digital Equipment Corp., Marlboro, MA) using dedicated array processors employing standard reconstruction algorithms. Images were transferred to SUN 3/60 workstations for further analysis. Image manipulations were performed using the ANALYZE software package (Mayo Foundation, Rochester, MN).

Calculation of Blood Volume. Images of the $C^{15}O$ distribution were divided by the average blood radioactivity concentration (cps/ml) obtained from the venous blood samples. Here, a blood density of 1.06 (g/ml) was assumed. This operation provided the blood volume images, which have units of milliliters of blood per milliliters of pixel. It should be noted that this blood volume is slightly greater than that measured by the $H_2{}^{15}O$ fitting analysis (V_a), because V_a excludes venous blood volume.

Selection of Blood-Pool ROIs. Three ROIs of different size were positioned in both the LV and LA chambers. The smallest ROI was selected by tracing a contour at approximately 90% of the peak of the blood volume image. The medium size ROI was selected by tracing a contour at approximately 80% of the peak counts. The largest ROIs were defined by tracing a contour at approximately 70% of the peak counts. These ROIs were projected onto the dynamic $C^{15}O_2$ data set, and LV and LA time-activity curves were generated by linearly interpolating the mid scan points of each frame data.

Selection of Myocardial ROIs. Myocardial tissue ROIs were selected to cover two anatomical regions, the anterior wall and the lateral wall. The selection was made by tracing ROIs on multiple slices of the extravascular density images which were calculated by subtracting the blood volume images from the normalized transmission images (*12,13*). Each ROI was projected onto the dynamic $C^{15}O_2$ data, and a mean time-activity curve was generated by averaging individual time-activity curves from different planes.

Calculation of MBF. MBF, tissue fraction and the fractional arterial blood volume were calculated by nonlinear least-squares regression analysis of the $C^{15}O_2$ time-activity curve data. These three parameters were fitted using an LV curve with and without the value of β given from the blood volume measurement, as well as an LA curve without the value of β. As a reference, fitting was also performed using the arterial blood curves which were directly measured by the beta probe.

RESULTS

Figure 3 shows results of the simulation study, illustrating the effects of spillover of tissue radioactivity into the LV ROI on the calculated parameters of f, α and V_a. Since no difference was observed in the errors between the two input functions described in Figure 1, only one result has been plotted. Small recovery of the left ventricle causes systematic overestimation in the values of f and V_a, approximately 40% for $\beta = 0.7$. Values of α were underestimated, although the magnitude was not large, approximately -15% for $\beta = 0.7$.

Figure 4 shows results of the simulation study demonstrating effects of statistical noise in the input function on the calculated parameters of f, α and V_a. As the noise level

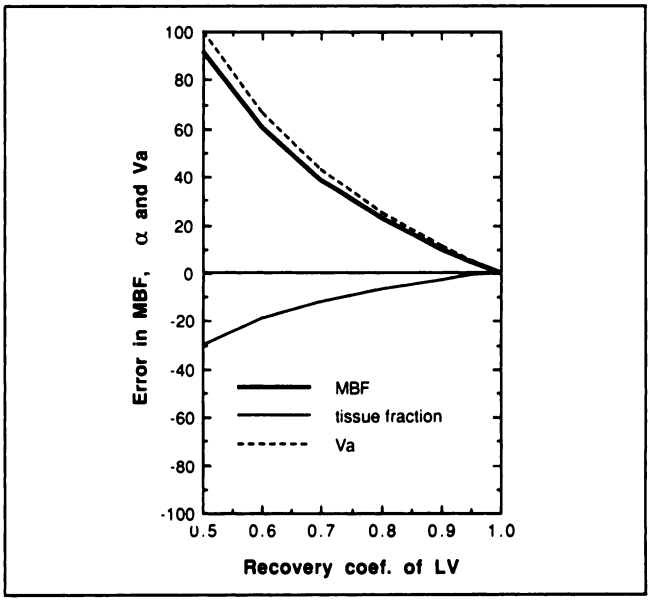

FIGURE 3. Results of the simulation studies demonstrating the effect of limited recovery of the LV counts on the calculated values of MBF (f), the tissue fraction (α) and the arterial blood volume (V_a). Since the simulation showed no difference in errors between the slow administration and the bolus administration procedures displayed in Figure 1, only one figure is plotted. The errors in each parameter are plotted as a function of the recovery coefficient of the LV counts (β). See also Figure 1 to compare these errors with the change in shape of the LV time-activity curves for various betas.

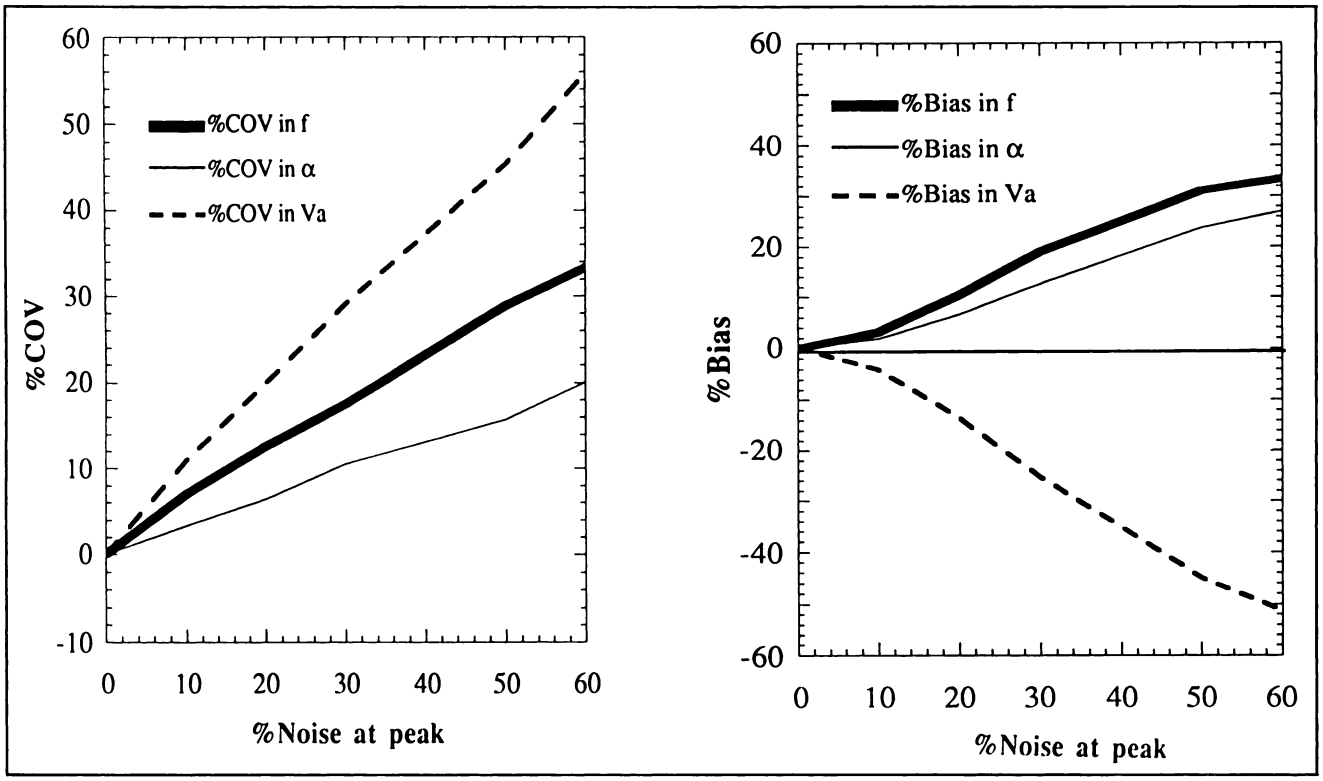

FIGURE 4. Results of the simulation studies demonstrating the effect of statistical noise in the input function on the calculated values of MBF (f), tissue fraction (α) and arterial blood volume (V_a). (A) Statistical fluctuation (%coefficient of variation in the calculated parameters) and (B) systematic bias (%difference between calculated and expected parameters) are plotted as a function of the assumed noise level (%standard deviation of the Gaussian distribution at peak of the input function). As statistical noise in the input function increases, both systematic bias and the statistical fluctuation increase in the calculated parameters.

increases, statistical fluctuation in the calculated parameters increases (Fig. 4A). In addition, systematic bias was caused by the statistical noise (Fig. 4B). The noise levels of 20%, 40% and 60% produce statistical fluctuations of 10%, 20%, and 30%, and systematic biases of 8%, 25% and 34% in estimation of MBF, respectively.

Figure 5 shows results of the simulation study, illustrating the effects of errors in measurement of the recovery coefficient of LV (β) on the calculated parameters of f, α and V_a. The error in each parameter increases almost linearly as the error in β increases. An error of ±10% in the measurement of β corresponds to an error of ±10% for MBF and V_a and ±4.5% for α.

Figure 6 illustrates an example of the comparison of input functions from a typical study during $C^{15}O_2$ inhalation. The three curves correspond to the beta-probe curve with correction for delay and dispersion (measured a(t)), the LV time-activity curve and the simulated arterial curve which was obtained by applying Equation 6 to the measured LV curve. The LV curve was systematically lower than the beta-probe curve during the administration period (build-up phase), but was similar during the post-administration period (wash-out phase). The simulated $a(t)$ curve reproduced the beta-probe curve well. The slight discrepancy between the measured and simulated a(t) curves around the peak is probably due to the limited sampling interval (30 sec) in measurement of the LV time-activity curve.

By using the beta-probe curves, the present study yielded average resting values of MBF (mean ± 1 standard devia-

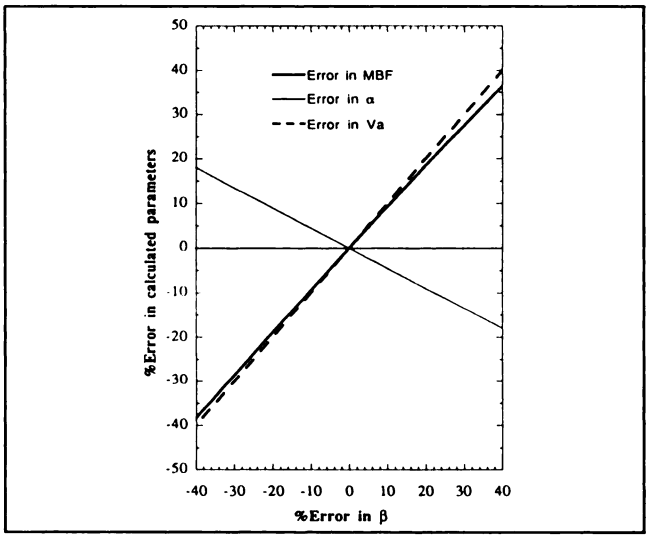

FIGURE 5. Results of the simulation studies demonstrating the effects of errors in the measurement of the recovery coefficient of LV (β) on the calculated values of MBF (f), the tissue fraction (α) and the arterial blood volume (V_a).

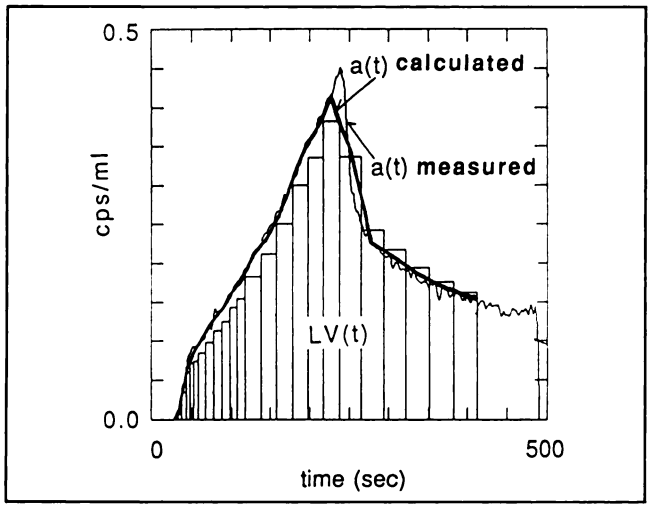

FIGURE 6. Comparison of three input functions obtained from a typical animal study using $C^{15}O_2$ inhalation. The histogram indicates the observed LV time-activity curve for ROIs of the largest size ($LV(t)$), the thin solid lines indicate the input functions directly measured using the beta probe after corrections for delay, dispersion and deadtime losses (measured $a(t)$), and the bold solid line indicates the predicted true input function calculated according to Equation 6 using the observed LV curves (calculated $a(t)$). The recovery coefficient of LV counts (β) was 0.746, as measured by a $C^{15}O$ blood volume scan, and MBF (f) was 1.07 ml/min/g.

tion): 0.90 ± 0.29, 1.05 ± 0.27 and 1.00 ± 0.25 ml/min/g and tissue fraction: 0.84 ± 0.04, 0.86 ± 0.13 and 0.97 ± 0.08 g/ml corresponding to the anterior, lateral and the septal regions, respectively. These resting MBF values were in agreement with our previous study performed on greyhounds (*5*). The tissue fraction values were consistently higher than the extravascular density values, which were calculated by subtracting the blood volume from a normalized transmission scan (*12,13*). Extravascular tissue density values were 0.81 ± 0.04, 0.76 ± 0.07 and 0.77 ± 0.05 g/ml corresponding to the above three regions, respectively. This observation was consistent with our previous finding (*14*) and has been explained by the myocardial venous blood volume.

Recovery coefficients for the LV ROIs (β) were 0.96 ± 0.03, 0.88 ± 0.06 and 0.76 ± 0.06 corresponding to the smallest, the medium and the largest ROIs, respectively. For these ROIs, the number of pixels included were 64 ± 22, 319 ± 98 and 517 ± 143, respectively (size of each pixel was 2 × 2 mm^2). Recovery coefficients for the LA ROIs (β) were 0.96 ± 0.03, 0.90 ± 0.08 and 0.83 ± 0.08, respectively. For these ROIs, the number of pixels included were 80 ± 19, 185 ± 42, and 321 ± 87, respectively.

Figure 7 shows the difference between MBF values calculated using the LV input function with those using the beta-probe analysis as a function of the recovery coefficient of the LV ROI. As the size of the LV ROI increases, which causes decreases in β, a systematic overestimation in the simulation of MBF increases when the present model is not applied. This overestimation in MBF is in agreement with the simulation studies. For small ROIs, the recovery coefficients were almost maximum ($\beta \geq 0.95$), and overestimation was smaller than for large ROIs. However, there was greater statistical fluctuation in MBF values (and in LV curves), and a systematic overestimation was also observed compared with the beta-probe analysis (7.7% ± 4.6%, $p < 0.02$ for $\beta > 0.95$).

When the tissue spillover correction was applied to the LV curves, the overestimation was removed for the large ROIs (small βs) as shown in Figure 7, and MBF values agreed well with those calculated by the beta-probe analysis. The maximum discrepancy in MBF was 2% for $\beta <$ 0.8. However, there was a significant correlation between the recovery coefficient (x-axis) and %difference in the MBF values calculated with the present model (y-axis), i.e., $y = 0.217x - 0.162$, $r = 0.518$, $p < 0.05$. This indicated that an overestimation in MBF remained for small ROIs (high recovery coefficient), even when the present model was used.

Figure 8 shows the difference between MBF values calculated using the LA input function with those by the beta-probe analysis as a function of the recovery coefficient of the LA ROI. MBF values were also overestimated for small βs (large ROIs) in comparison to the beta-probe

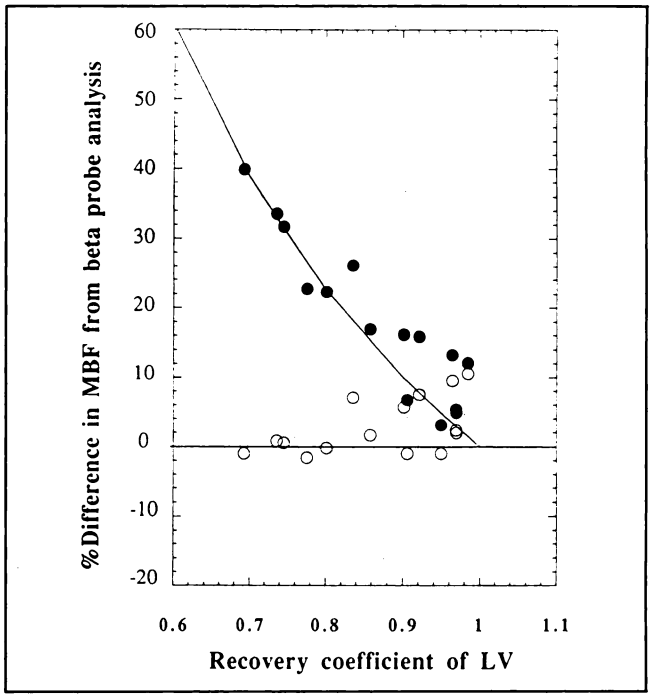

FIGURE 7. Difference of MBF values obtained by use of LV curves from those calculated using the beta-probe curves. Data are plotted as a function of the recovery coefficient (β) of each LV ROI. Closed circles correspond to MBF values calculated using the directly measured LV curves as input functions (replacing $\alpha(t)$ by $LV(t)$ and fitting with Equation 3). Open circles indicate results after correction of the $LV(t)$ curve by the model (fitting of Equation 5 using $LV(t)$ with given values of β obtained from the $C^{15}O$ blood volume measurement). The solid line indicates the error in MBF with varying β from the simulation studies.

analysis when LA curves were used directly as input functions (+8% for $\beta > 0.9$). The overestimation was not as large as that for the LV ROIs. For small LA ROIs (e.g., $\beta > 0.95$), a small but significant overestimation was observed compared with the beta-probe analysis [4.3 ± 3.5% ($p < 0.05$)].

DISCUSSION

Use of the LV Input Function

Use of the LV time-activity curve obviates the need for arterial cannulation for MBF measurement using $H_2{}^{15}O$ and dynamic PET imaging. However, one of the limitations of this approach is the spillover of tissue radioactivity into the input function curve, which is due to the limited recovery of the LV counts caused by cardiac motion and the small size of the ventricular chamber. This spillover of surrounding tissue activity causes distortion of the input function (Fig. 1) and hence significant overestimation in the calculated MBF values, as illustrated in Figures 3 and 7. As can be seen from Figures 1 and 3, only small differences in the shape of the input function cause significant systematic errors (systematic overestimation) in the calculated MBF values. Consequently, systematic differences between subject groups may result. For example, higher than normal MBF values would be expected in patients with smaller hearts than in normal subjects. The present investigations using greyhounds provided almost maximum recovery coefficients by carefully selecting a small ROI in the LV chamber. In human studies, however, it may be more difficult to find LV ROIs with such large recovery coefficients, because ventricular size in a human is usually smaller than that of a greyhound (*5*).

Another limitation in the use of the LV curve is related to limited counting statistics. The present simulation study demonstrated that the statistical noise in the input function causes systematic bias in the calculated parameters (overestimation in f and α, and underestimation in V_a) in addition to the increased statistical fluctuation. The effect of the statistical noise in the input function is probably more serious in human studies than in the present greyhound studies, because attenuation is greater in humans than in smaller animals. Thus, selecting a larger ROI or performing a smoothing operation on the original dynamic images is needed to minimize statistical fluctuation in the noninvasive input function. However, both procedures increase "contamination" from tissue radioactivity, resulting in systematic overestimation in calculated MBF values.

The present model corrects for spillover of tissue radioactivity into the LV input function and thus provides a solution for the limitations described above. This method requires measurements of the LV time-activity curve during the dynamic $H_2{}^{15}O$ scan and the recovery coefficient of the LV (β). Here, the determination of β can be achieved simply by sampling venous blood during the $C^{15}O$ blood volume scan, thus eliminating the need for arterial blood sampling. As has been demonstrated in Figures 6 and 7, this model has been validated with regard to its ability to reproduce the true input function and to provide equivalent values of MBF in comparison to beta-probe analysis following arterial cannulation.

The largest ROIs selected on the LV regions include approximately eight times more pixels in comparison to the smallest ROIs, which corresponds to an improvement in the statistical fluctuation by a factor of approximately three in each time point of the LV curve. This is equivalent to the averaging operation for eight time-activity curves for small ROIs that are obtained from different PET planes. Selection of one ROI on a single plane is practically easier than carefully drawing multiple ROIs on different planes. However, when applying this method to human subjects, it may be necessary to select multiple, large ROIs on different PET planes and to calculate the average of the individual time-activity curves, since the attenuation will be greater than that in the greyhounds used in this study.

The present model also includes the concept of the tissue fraction (*5*). This parameter has been defined as the mass of perfusable tissue per volume of the ROI (g/ml) correcting for the limited recovery in the measurement of tissue radioactivity. Thus, this model implements partial volume corrections to both the myocardial tissue curves and the LV time-activity curve.

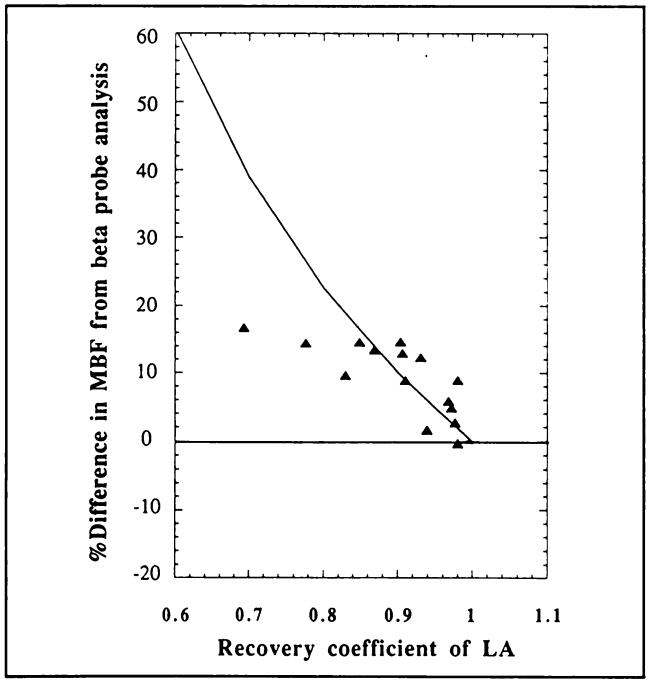

FIGURE 8. Difference of MBF values obtained by use of LA curves from those calculated using the beta-probe curves. Data are plotted as a function of the recovery coefficient (β) of each LA ROI. Triangles correspond to MBF values calculated using the directly measured LA curves as input functions. The solid line indicates the error in MBF with varying β from the simulation study for an LV input function.

Use of the LA Input Function

It is reasonable that the LA time-activity curves, when compared to LV ROIs, have a smaller spillover component from surrounding tissue due to the thickness of the LA wall. Our data confirmed that direct use of the LA curve for the input function provided less error (overestimation) in MBF than the LV curve, when not incorporating the present model. However, MBF values were still significantly greater than those obtained with the beta-probe analysis. As shown in Figure 8, the overestimation was 4.3% ± 3.5% in MBF for high recovery ($\beta > 0.95$), and it increased almost linearly as the recovery coefficient decreased (approximately 20% for $\beta \approx 0.7$). This overestimation in MBF for low recovery (approximately half of that using the uncorrected LV input function) may be due to spillover of radioactivity from the LA wall, the LV wall or the lung regions. The overestimation for large recovery (small ROIs) may be due to the limited count statistics, as demonstrated by the simulation study (Fig. 4B).

It might therefore be advantageous to draw several ROIs for the LA region on different planes in order to calculate an average LA curve. However, more statistical noise can be expected in human studies because of larger attenuation in the body of the human subject, and hence, calculated MBF values could still be overestimated as indicated by the simulation (Fig. 4B) in addition to increased statistical fluctuation. Further studies are required to evaluate errors in humans due to statistical noise in the input function.

The use of the present model may be limited in correction for LA curves. It should be noted that in Figure 8 the measured values of MBF using an LA input function do not correspond well with the results of the simulation studies. This is probably due to the inadequacy of assumption 4 described in Materials and Methods.

It should also be noted that the MBF value calculated using the LA input function does not change even if the LA curve is simply divided by β, because MBF is calculated from the clearance of $H_2{}^{15}O$ from the myocardium in the present model and is not sensitive to the scaling factor of the input curve (see Equation 3).

Limitations of the Model

In the present model, a homogeneous distribution of MBF throughout the ventricular wall was assumed. This assumption, however, will be invalid in patients with focal abnormalities in their MBF distribution. In such patients, it would be better to first calculate the true input function by selecting a ROI that covers the entire ventricular wall, fit the LV and resulting whole myocardial time-activity curves using Equation 5, and then calculate the true input function using Equation 6 to give a mean value of MBF. Regional MBF values may then be calculated for each myocardial segment using the predicted true input function. Further study is required to confirm the validity of this approach.

Great accuracy is required in measuring the LV time-activity curve because only a small change in the shape causes serious errors in the final MBF value (Figs. 1 and 3). A slow administration protocol would be preferable to a bolus administration in order to minimize errors in the measurement of the LV curve due to the smaller corrections for deadtime losses and random coincidence events. For the slow administration protocol, three parameters are fitted, V_a, MBF and α, despite the blood volume data being available for measurement of recovery coefficient, β. This is because the $C^{15}O$ blood volume data overestimates the arterial blood contribution (V_a) when correcting for spillover of blood radioactivity into the tissue ROI. In contrast, for the bolus administration protocol, two parameters are fitted, MBF and tissue fraction; the error due to blood volume subtraction is minimized by masking the early portion of the tissue curve, as has been demonstrated (*4*). It may be possible to reduce the number of fitted parameters for the slow administration protocol by introducing the venous blood volume into the model, because the change in the venous blood volume is small compared with the change in total blood volume even after drug intervention (*14,15*). Further study is needed to confirm this.

Errors in MBF, α and V_a, are independent of the shape of the true input function (i.e., independent of the tracer administration procedure), which were tested for two different input functions shown in Figure 1. This indicated that errors due to the limited recovery cannot be reduced by only changing the administration procedure.

There may be an upper size limit in the present method when selecting a LV ROI to provide the input function, because of the assumption $\beta + \gamma = 1$. This assumption may not be valid for extremely large ROIs, even though statistical accuracy is improved. We have confirmed that this approach was valid for $\beta > 0.7$ in greyhounds. However, it is important to test this in human studies.

Future Applications

The present study suggests that a noninvasive input function can be obtained by scanning the LV chamber. This may also be applicable to brain studies if an additional PET detector ring is available so that the heart can be scanned simultaneously with the brain. This second ring does not necessarily require the same high spatial resolution as that of current neuro PET scanners, nor such high sensitivity. However, it may need high counting rate characteristics to collect sufficient counts within a limited time.

The model presented in this study, which corrects for loss of counts in the vascular ROI and spillover of radioactivity from surrounding tissue into the vascular ROI, may be generally applicable to other locations such as the radial artery by scanning the wrist and the carotid artery by scanning the neck. The most important limitation may be related to the fourth assumption listed in Materials and Methods (i.e., $\beta + \gamma = 1$) (*16*). Further studies are required to assess these possibilities.

The present model should be applicable to other kinetic studies with other tracers such as ^{18}F-fluoro-deoxyglucose

and ^{13}N-ammonia, as long as the behavior of the tracer in the myocardium can be related, in mathematical terms, to the whole blood and not to the plasma time-activity curve.

ACKNOWLEDGMENTS

The authors thank Miss C.J.V. Taylor and Mr. G. Lewington for technical support, Mr. D. Wilson for assistance with the animal preparation, and J. Ashburner and J.D. Heather for computer assistance. H.I., a visiting scientist from the Research Institute for Brain and Blood Vessels, Akita, Japan, is supported by the Japan Heart Foundation and a 1988 Bayer Yakuhin grant. R.D.S. is a postgraduate student in the MRC Cyclotron Unit and Division of Biomedical Sciences (Physiology Group), King's College London. He is a recipient of an MRC postgraduate research studentship. This work was presented in part at the 37th Annual Meeting of the Society of Nuclear Medicine, Washington, DC, 1990.

REFERENCES

1. Kanno I, Lammertsma AA, Heather JD, et al. Measurement of cerebral blood flow using bolus inhalation of $C^{15}O_2$ and positron emission tomography: description of method and its comparison with the $C^{15}O_2$ continuous inhalation method. *J Cereb Blood Flow Metab* 1984;4:224–234.
2. Iida H, Kanno I, Miura S, Murakami M, Takahashi K, Uemura K. Error analysis of a quantitative cerebral blood flow measurement using $H_2{}^{15}O$ autoradiography and positron emission tomography, with respect to the dispersion of the input function. *J Cereb Blood Flow Metab* 1986;6: 536–545.
3. Weinberg IN, Huang SC, Hoffman EJ, et al. Validation of PET-acquired input functions for cardiac studies. *J Nucl Med* 1988;29:241–247.
4. Iida H, Kanno I, Takahashi A, et al. Measurement of absolute myocardial blood flow with $H_2{}^{15}O$ and dynamic positron-emission tomography: strategy for quantification in relation to the partial-volume effect. *Circulation* 1988;78:104–115.
5. Araujo LI, Lammertsma AA, Rhodes CG, et al. Non-invasive quantification of regional myocardial blood flow in normal volunteers and patients with coronary artery disease using oxygen-15 labelled water and positron emission tomography. *Circulation* 1991;83:875–885.
6. Bergmann SR, Herrero P, Markham J, et al. Noninvasive quantitation of myocardial blood flow in human subjects with oxygen-15-labeled water and positron emission tomography. *J Am Coll Cardiol* 1989;14:639–652.
7. Kety SS. The theory and applications of exchange of inert gas at the lungs and tissues. *Pharmacol Res* 1951;3:1–41.
8. Kety SS. Measurement of local blood flow by the exchange of an inert, diffusible substance. *Methods Med Res* 1960;8:228–236.
9. Konno O, Simano K. *Biochemical data.* Tokyo: Igaku-Shoin; 1965:440–441.
10. Spinks TJ, Jones T, Gilardi MC, Heather JD. Physical performance of the latest generation of commercial positron scanner. *IEEE Trans Nucl Sci* 1988;35:721–725.
11. Spinks TJ, Araujo LI, Rhodes CG, Hutton BF. Physical aspects of cardiac scanning with a block detector positron tomograph. *J Comput Assist Tomogr* 1991: in press.
12. Rhodes CG, Wollmer P, Fazio F, Jones T. Quantitative measurement of regional extravascular density using positron emission and transmission tomography. *J Comput Assist Tomogr* 1981;5:783–791.
13. Iida H, Rhodes CG, De Silva R, Yamamoto Y, Jones T, Araujo LI. Myocardial tissue fraction—correction for partial volume effects and measure of tissue viability. *J Nucl Med* 1991;32:2169–2175.
14. Crystal GJ, Downey HF, Bashour AFA. Small vessel and total coronary blood volume during intracoronary adenosine. *Am J Physiol* 1981;241:H194–H201.
15. O'Keefe DD, Hoffman JIE, Cheitlin R, O'Neill MJ, Allard JR, Shapkin E. Coronary blood flow in experimental canine left ventricular hypertrophy. *Circ Res* 1978;43:43–51
16. Henze E, Huang SC, Ratib O, Hoffman E, Phelps ME, Shelbert HR. Measurement of regional tissue and blood radiotracer concentrations from serial tomographic images of heart. *J Nucl Med* 1983;24:987–996.